Communication

Fabrication of ZnO "Dandelions" via a Modified Kirkendall Process

Bin Liu, and Hua Chun Zeng

More About This Article

Additional resources and features associated with this article are available within the HTML version:

- Supporting Information
- Links to the 60 articles that cite this article, as of the time of this article download
- Access to high resolution figures
- Links to articles and content related to this article
- Copyright permission to reproduce figures and/or text from this article

View the Full Text HTML

Fabrication of ZnO "Dandelions" via a Modified Kirkendall Process

Bin Liu and Hua Chun Zeng*

*Department of Chemical and Biomolecular Engineering, Faculty of Engineering, National University of Singapore,
10 Kent Ridge Crescent, Singapore 119260*

Received August 26, 2004; E-mail: chezhc@nus.edu.sg

The Kirkendall effect normally refers to comparative diffusive migrations among different atomic species in metals and/or alloys under thermally activated conditions.[1] Because of the difference in atomic diffusivities, for example, zinc diffuses into the copper faster than the copper diffuses into the brass in a brass−copper interface.[1] A common result form this process is generation of porosity in the lower-melting component side of the diffusion couple. While metallurgists have tried for decades to prevent void formation in alloys and solders, nonetheless, the directional matter flow and consequential vacancy accumulation may provide possibilities for chemists to design and synthesize new materials. Very recently, a process analogous to the Kirkendall phenomenon has been successfully developed for nanoscale fabrication of a variety of hollow crystals, including yolk-shell metal−metal-oxide structures.[2] Herein, we will further demonstrate that the Kirkendall-type mass transport, when coupled with interfacial reactions, can be utilized in synthetic nanoarchitecture, through which individual building components can be designed and organized chemically into complex geometrical conformations. As a first example, single-crystalline zinc oxide (ZnO) nanorods or nanoplatelets have been aligned into curved arrangements analogous to the "parachutes" array in a dandelion. This method may provide a new synthetic alternative to materials self-organization.[3−16] It should also be mentioned that the ZnO chosen in this work has attracted great attention in recent years, and various structural and morphological investigations have been carried out in addition to its property studies.[8,9,17,18]

In our experiments, 0.065−0.65 g (1−10 mmol) of metallic zinc powder in spherical shape was added to 0−25 mL (mostly 25 mL) of deionized water under stirring at room temperature to ensure well dispersion of the powder. A zincate ion (ZnO_2^{2-}) solution (0−30 mL, mostly 5 mL; [$Zn(NO_3)_2$] = 0.5 M and [NaOH] = 5.0 M) was then added while the stirring continued. Afterward, the mixture was transferred to a Teflon-lined stainless steel autoclave and kept inside an electric oven at 100−200 °C for 2−24 h. After synthesis, the ZnO products were washed several times with deionized water and pure ethanol and collected by sedimentation. The collected samples were then vacuum-dried. The crystal phase was determined with powder X-ray diffraction (XRD, Shimadzu XRD-6000, Cu Kα radiation). The structural and compositional information of the product materials was obtained with field-emission scanning electron microscopy (FESEM, JSM-6700F), transmission electron microscopy and selected area electron diffraction (TEM/SAED, JEM-2010F), high-resolution TEM and energy-dispersive X-ray spectroscopy (HRTEM/EDX, Tecnai-G², FEI), and X-ray photoelectron spectroscopy (XPS; AXIS-HSi, Kratos Analytical). Deposition of Au nanoparticles onto the prepared ZnO was also carried out, and optical properties of the Au−ZnO nanocomposites were investigated with a UV−vis−NIR scanning spectrophotometer (Shimadzu UV-3101PC).
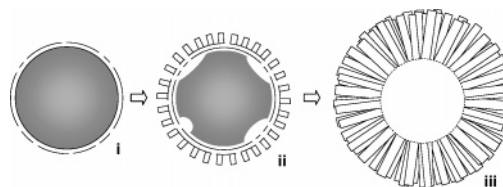

Figure 1. Schematic illustration of formation of ZnO dandelions: (i) metallic Zn (gray core) with its surface oxide (white shell), (ii) modified Kirkendall process through surface oxide region and ZnO nucleation, and (iii) continuous evacuation of Zn core and growth of ZnO nanorods.
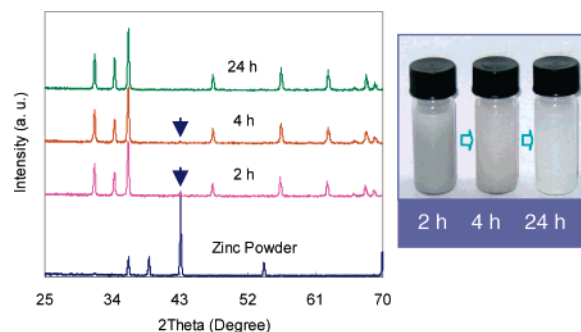

Figure 2. Evolution of XRD patterns from Zn powder to ZnO dandelions (green, red, and pink patterns belong to ZnO while the one in blue belongs to the as-received metallic Zn). A small diffraction peak of the metallic Zn (marked with blue arrows) can still be seen in the ZnO samples synthesized for 2 and 4 h, which is consistent with their color changes of the corresponding suspensions (dispersed in ethanol solvent), from light gray to white after reactions at 180 °C (the photograph on the right).

Figure 1 depicts the synthetic flowchart of this work. Different from the conventional Kirkendall process, our process is modified with additional solution reactions:

$$Zn + 2OH^- \rightarrow ZnO_2^{2-} + H_2 \qquad (1)$$

$$ZnO_2^{2-} + H_2O \leftrightarrow ZnO + 2OH^- \qquad (2)$$
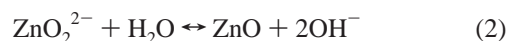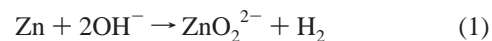
where diffusing Zn atoms at liquid−solid interface turn into soluble zincate ions ZnO_2^{2-}, after which the anions react with water and deposit back to the solid phase (ZnO). The spherical Zn powder has a diameter in the range of 2−12 μm (Supporting Information (SI)-1). In most of our experiments, the metallic Zn powder can be largely converted to ZnO within a short reaction time (e.g., 180 °C, 2 h; Figure 2). The dissolution of Zn also occurs at <100 °C and 1 atm, and H_2 bubbles can be seen directly through a transparent reactor. Because H_2 is released, reaction 1 is irreversible, which provides an additional driving force for Zn out-diffusion from the metal cores.

Our XRD study in Figure 2 shows that all the prepared ZnO samples are in wurtzite phase (space group: $P6_3mc$; JCPDS card no. 36-1451),[8,18] and the lattice constants of this hexagonal phase c_o and a_o are 5.21 and 3.25 Å, respectively.
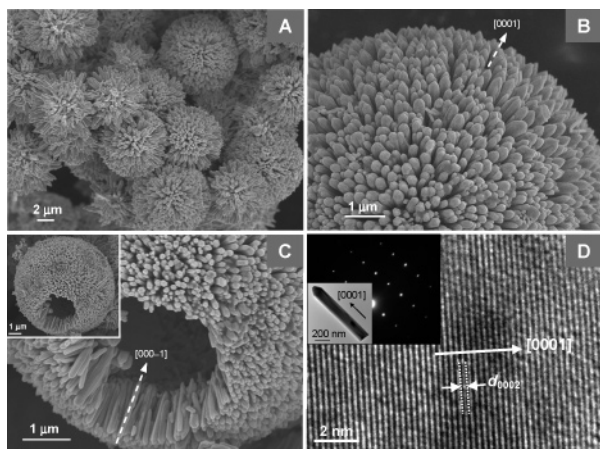
Figure 3. FESEM images (A−C) of ZnO dandelions (180 °C, 24 h). (A) Overall product morphology. (B, C, and inset) Detailed shell structures assembled by ZnO nanorods. (D) SAED (inset) and a HRTEM image.
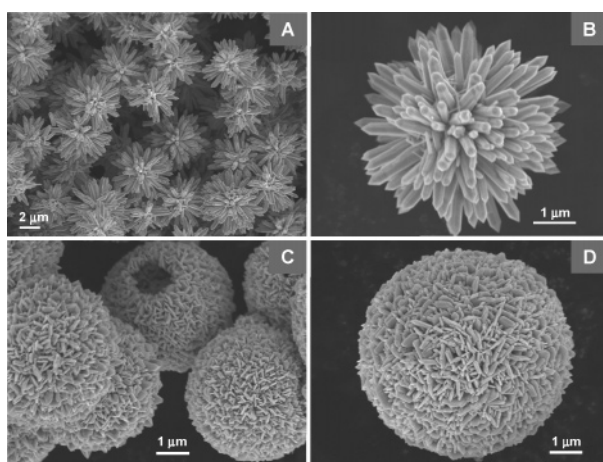

Figure 4. FESEM images of ZnO dandelions prepared from small Zn metal balls (A and B, 180 °C, 2 h), and hollow ZnO dandelions prepared at higher temperatures (C and D, 200 °C, 4 h).

As shown in Figure 3, the ZnO "dandelions" comprise numerous one-dimensional nanorods with their −c-axes ([000−1]; SAED) pointing toward the center of dandelion sphere (Figure 3A−C). The diameter and length of these nanorods are in the ranges of 100−300 nm and 1−4 μm, respectively, depending on the synthetic conditions. For example, the thickness of ZnO shell (equal to the nanorod length) in Figure 3C is estimated to be about 1.5−2 μm. With this approach, a large central space can be created (see a cracked opening, Figure 3C). Individual ZnO nanorods are single crystalline, as revealed in the diffraction pattern of the [1−100] zone spots (Figure 3D) and shown in the hexagonal prismatic facets and clear lattice fringes of d_{0002} (2.6 ± 0.1 Å; Figure 3D).[8,18] Furthermore, our EDX measurement affirms a strict stoichiometric ratio of Zn:O = 1:1 (SI-2) for the prepared ZnO. The product morphology of this type can be easily controlled; a 100% of morphological yield of ZnO dandelions with interior space had been achieved in this work (SI-3).

Our synthetic parameters allow further structural manipulation. In addition to the large dandelions, for example, smaller ZnO dandelions consisting of fewer nanorods can also be prepared with a shorter reaction time, as displayed in Figure 4A,B. This crystal morphology was formed from small-sized pristine Zn balls (SI-1), and a high morphological yield can also be attained with a sedimentation separation (100%, SI-4). Nonetheless, they were metastable and readily converted to the larger ones (i.e., Figure 3)
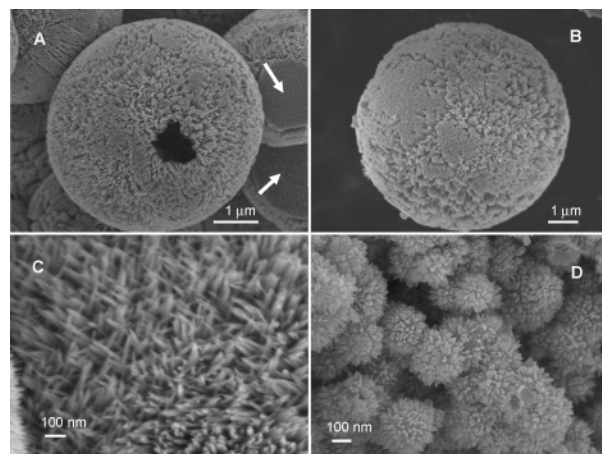
Figure 5. FESEM images of ZnO dandelions prepared at room temperature. (A and B) With large Zn particles (5−12 μm). (D) With small Zn particles (150−200 nm). (C) General surface structure of the hollow spheres in (A and B). Experimental conditions: 25 °C for 4 h.
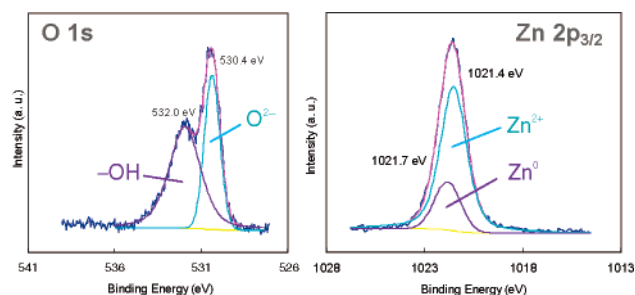

Figure 6. O 1s and Zn 2p$_{3/2}$ XPS spectra of as-received Zn particles.

upon a longer reaction time due to Ostwald ripening. At higher temperatures, on the other hand, platelet-like ZnO building units can be prepared in constructing another type of dandelions (also with hollow interiors, Figure 4C,D). The platelets in the shell were grown from a lateral elongation along the ⟨11−20⟩ directions of nanorods while keeping their c-orientation unchanged (still perpendicular to the spheres, 100% morphological yield; SI-5).

Similar to those synthesized at 100−200 °C, core hollowing can also take place at room temperature. Figure 5 shows some of our results using two different sizes of metallic zinc particles. In general, much finer but less perpendicular ZnO nanorods were obtained at lower temperatures (Figure 5C). In certain areas, c-oriented flat domains were formed (indicated with white arrows; Figure 5A), which implies that, unlike the previous cases, the common center is no longer held for all the nanorods of the shells. As a further extension of the present work, pristine Zn particles with a size distribution of 150−200 nm were also tested for ZnO formation. Once again, similar dandelion-like ZnO can be obtained but at a much smaller size range (250−350 nm; Figure 5D); their hollow interiors were also affirmed (SI-6).

Dandelion-like conformation had been recently fabricated for CuO, on the basis of geometrical constraints of starting building blocks (each building unit in turn was formed in situ from individual CuO nanoribbons via a "oriented attachment" process, or a "growth-then-assembly" method).[16] The approach of Figure 1, in contrast, belongs to a "growth-cum-assembly" process. It has been revealed that the preformed ZnO oxide layer on the pristine Zn powder is crucial to the success of initial nucleation and subsequent deposition of ZnO. In Figure 6, binding energies of Zn 2p$_{3/2}$ photoelectrons of Zn^{2+} and O 1s photoelectrons of O^{2-} were measured at 1021.4 and 530.4 eV, respectively.[19] This XPS analysis reveals that ZnO
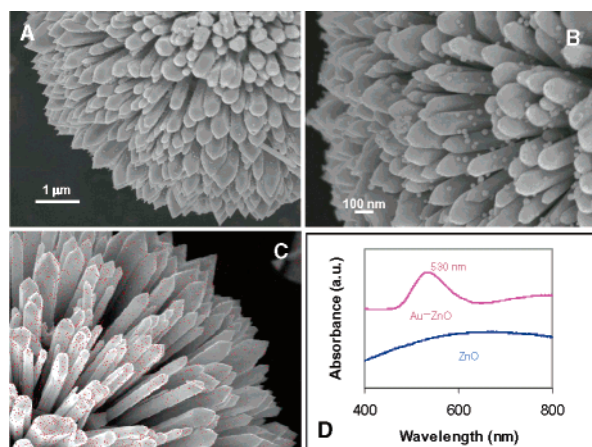
Figure 7. (A and B) FESEM images of Au−ZnO composite dandelions. (C) FESEM image with Au element mapping in red dots. (D) UV−vis spectra of ZnO and Au−ZnO dandelion suspensions (in ethanol). Experimental condition: 0.1 g of ZnO dandelions in 20 mL of H_2O + 1.0 mL of 0.01 M sodium citrate + 1.0 mL of 0.01 M $HAuCl_4$ + 2.0 mL of 0.01 M ascorbic acid at room temperature for 5 min.
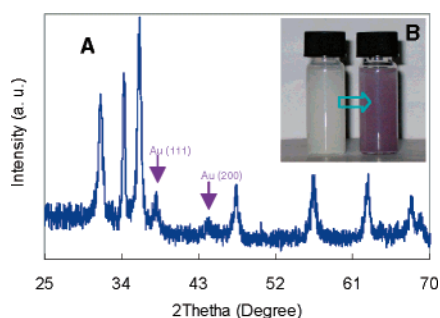

Figure 8. (A) XRD patterns of ZnO (unmarked in blue) and Au (marked with the purple arrows) for an Au−ZnO composite. (B) Color change upon the Au deposition (dispersed in ethanol): ZnO dandelions (white) to the Au−ZnO composite dandelions (purple).

is a predominant surface phase on the as-received Zn powder. In our modified Kirkendall process, introduction of ZnO_2^{2-} to the starting solution is a prerequisite to protect this layer (i.e., to prevent the equilibrium (2) from shifting to the left). Our experiments have showed that this oxide layer was destroyed in absence of initial ZnO_2^{2-}; incomplete dandelions were formed (SI-7). Nonetheless, an exceedingly high concentration of starting ZnO_2^{2-} would promote the spontaneous nucleation in solution and thus eliminate the desired shell growth (SI-7), giving unorganized rodlike ZnO products. In a broader sense, therefore, one can consider that an overall ZnO dandelion conformation is "sculptured" chemically from a single piece of raw material (i.e., a single Zn ball). As a further confirmation, the intermediate structure of Figure 1ii has been indeed found in our experiments with a short reaction time (e.g., 180 °C, 2 h; SI-8).

In addition to the above morphological controls, composition of the prepared ZnO dandelions can still be tailored. As an example, Figures 7 and 8 show such a synthetic flexibility in fabricating Au−ZnO nanocomposite where Au nanospheres (5−25 nm) have been evenly deposited onto the surfaces of nanorods, as indicated in Figure 7A−C (element mappings: SI-9). Interestingly, the tips of nanorods are also decorated with Au nanoparticles (i.e., Au on the (0002) planes of ZnO; SI-10). The resultant Au−ZnO shows a distinct color change (Figure 8). Consistent with this, a surface

plasma resonance peak of Au is observed at ca. 530 nm (Figure 7D), apart from the UV absorption of ZnO at 373 nm (not shown).[18] One of the structural features of these dandelion-like materials is that one- or two-dimensional building blocks (anisotropic) can be selectively made and aligned into highly symmetrical three-dimensional conformations (isotropic), which may promise us new types of applications. For example, this class of metal-oxides and metal-semiconductor composites should be potentially useful for applications such as storage of light-generated electrons,[20] three-dimensional lasing,[9] and new ways of photocatalysis.[17,18]

In summary, micrometer- and submicrometer-scale hollow ZnO dandelions with single-crystalline building units (either nanorods or nanoplatelets) can be constructed via a modified Kirkendall process in solution, where the preformed oxide layer serves as a shell template for the initial nucleation and growth. In principle, a great variety of oxide dandelions and their nanocomposites can be fabricated through this type of total synthetic architecture.

Supporting Information Available: EDX, SEM, FESEM, and TEM results. This material is available free of charge via the Internet at http://pubs.acs.org.

References

(1) (a) Kirkendall, E.; Thomassen, L.; Upthegrove, C. *Trans. AIME* **1939**, *133*, 186−203. (b) Kirkendall, E. O. *Trans. AIME* **1942**, *147*, 104−110. (c) Smigelskas, A. D.; Kirkendall, E. O. *Trans. AIME* **1947**, *171*, 130−142.
(2) Yin, Y.; Rioux, R. M.; Erdonmez, C. K.; Hughes, S.; Somorjai, G. A.; Alivisatos, A. P. *Science* **2004**, *304*, 711−714.
(3) (a) Whitesides, G. M.; Grzybowski, B. *Science* **2002**, *295*, 2418−2421. (b) Thalladi, V. R.; Whitesides, G. M. *J. Am. Chem. Soc.* **2002**, *124*, 3520−3521. (c) Wu, H.; Thalladi, V. R.; Whitesides, S.; Whitesides, G. M. *J. Am. Chem. Soc.* **2002**, *124*, 14495−14502.
(4) (a) Smith, P. A.; Nordquist, C. D.; Jackson, T. N.; Mayer, T. S.; Martin, B. R.; Mbindyo, J.; Mallouk, T. E. *Appl. Phys. Lett.* **2000**, *77*, 1399−1401. (b) Kovtyukhova, N. I.; Mallouk, T. E. *Chem.−Eur. J.* **2002**, *8*, 4355−4363.
(5) (a) Love, J. C.; Urbach, A. R.; Prentiss, M. G.; Whitesides, G. M. *J. Am. Chem. Soc.* **2003**, *125*, 12696−12697. (b) Urbach, A. R.; Love, J. C.; Prentiss, M. G.; Whitesides, G. M. *J. Am. Chem. Soc.* **2003**, *125*, 12704−12705.
(6) Cölfen, H.; Mann, S. *Angew. Chem., Int. Ed.* **2003**, *42*, 2350−2365.
(7) Velikov, K. P.; Christova, C. G.; Dullens, R. P. A.; van Blaaderen, A. *Science* **2002**, *296*, 106−109.
(8) (a) Pan, Z. W.; Dai, Z. R.; Wang, Z. L. *Science* **2001**, *291*, 1947−1949. (b) Gao, P.; Wang, Z. L. *J. Phys. Chem. B* **2002**, *106*, 12653−12658. (c) Kong, X. Y.; Ding, Y.; Yang, R.; Wang, Z. L. *Science* **2004**, *303*, 1348−1351. (d) Gao, P. X.; Wang, Z. L. *J. Am. Chem. Soc.* **2003**, *125*, 11299−11305.
(9) Huang, M. H.; Mao, S.; Feick, H.; Yan, H.; Wu, Y.; Kind, H.; Webber, E.; Russo, R.; Yang, P. *Science* **2001**, *292*, 1897−1899.
(10) (a) Kim, F.; Kwan, S.; Akana, J.; Yang, P. *J. Am. Chem. Soc.* **2001**, *123*, 4360−4361. (b) Yang, P. *Nature* **2003**, *425*, 243−244.
(11) Caruso, F.; Caruso, R. A.; Möhwald, H. *Science* **1998**, *282*, 1111−1114.
(12) Sun, Y.; Xia, Y. *Science* **2002**, *298*, 2176−2179.
(13) Whang, D.; Jin, S.; Wu, Y.; Lieber, C. M. *Nano Lett.* **2003**, *3*, 1255−1259.
(14) Dinsmore, A. D.; Hsu, M. F.; Nikolaides, M. G.; Marquez, M.; Bausch, A. R.; Weitz, D. A. *Science* **2002**, *298*, 1006−1009.
(15) Park, S.; Lim, J.-H.; Chung, S.-W.; Mirkin, C. A. *Science* **2004**, *303*, 348−351.
(16) Liu, B.; Zeng, H. C. *J. Am. Chem. Soc.* **2004**, *126*, 8124−8125.
(17) (a) Tian, Z. R.; Voigt, J. A.; Liu, J.; Mckenzie, B.; Mcdermott, M. J. *J. Am. Chem. Soc.* **2002**, *124*, 12954−12955. (b) Pacholski, C.; Kornowski, A.; Weller, H. *Angew. Chem., Int. Ed.* **2004**, *43*, 4774−4777. (c) Li, F.; Ding, Y.; Gao, P.; Xin, X.; Wang, Z. L. *Angew. Chem., Int. Ed.* **2004**, *43*, 5238−5242 and references therein.
(18) (a) Liu, B.; Zeng, H. C. *J. Am. Chem. Soc.* **2003**, *125*, 4430−4431. (b) Liu, B.; Zeng, H. C. *Langmuir* **2004**, *20*, 4196−4204.
(19) (a) Futsuhara, M.; Yoshioka, K.; Takai, O. *Thin Solid Films* **1998**, *317*, 322−325. (b) Chang, S.-S.; Choi, G. J.; Park, H. J.; Stora, M. E.; Hummel, R. E. *Mater. Sci. Eng.* **2001**, *B83*, 29−34.
(20) Hirakawa, T.; Kamat, P. V. *Langmuir* **2004**, *20*, 5645−5647.

JA044825A